Fuel 279 (2020) 118321

Contents lists available at ScienceDirect

Fuel

journal homepage: www.elsevier.com/locate/fuel

Full Length Article

A study of droplet deformation: The effect of crossflow velocity on jet fuel and biofuel droplets impinging onto a dry smooth surface

Inês Ferrão[a,b,c], Daniel Vasconcelos[a], Daniela Ribeiro[a], André Silva[a,*], Jorge Barata[a]

[a] AEROG/LAETA, Universidade da Beira Interior, Covilhã, Portugal
[b] IN+/LARSyS, Instituto Superior Técnico, Universidade de Lisboa, Lisboa, Portugal
[c] IDMEC/LAETA, Instituto Superior Técnico, Universidade de Lisboa, Lisboa, Portugal

GRAPHICAL ABSTRACT

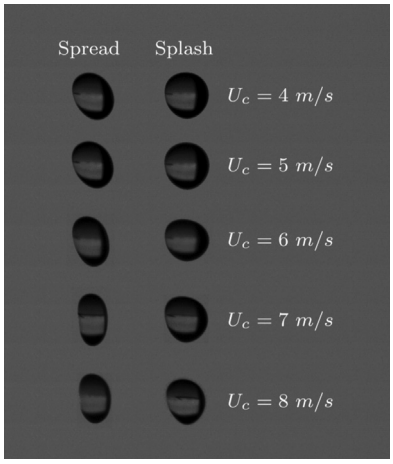

ARTICLE INFO

Keywords:
Droplet impact
Dry surface
Crossflow
Droplet deformation
Secondary atomisation

ABSTRACT

The aeronautical sector has been, in the last decade, one of those that most invested in more efficient and ecological solutions in order to reduce significantly greenhouse gas and pollutant emissions. The introduction of biofuels in fuel mixtures for aircraft engines is a promising alternative in this sector. The main objective of this experimental study is understanding the influence of crossflow variation on droplet deformation and consequent impact outcomes. An experimental facility was developed and validated to study the impact of single droplets onto a dry, smooth aluminium impact surface under the influence of several crossflow velocities. Different crossflow velocities of 4, 5, 6, 7 and 8 m/s were tested. A combination of conventional jet fuel and a biofuel was considered to understand the behavior of jet fuel and biofuel mixtures, and three fluids were used: 100% jet fuel, 75% jet fuel/25% biofuel and 50% jet fuel/50% biofuel. Several parameters, including velocity components, impact angle and eccentricity, were analysed for the different crossflow velocities, and the spread and splash regimes were also defined for the different fluids. The results display that, for each crossflow velocity, an increase in the droplet impact velocity causes a shift from the spread to the splash regime. The presence of a crossflow induces deformation on the droplet, altering its outcome. Ellipsoidal droplets promote the occurrence of spreading, whereas splashing tends to occur for spherical forms, corresponding to higher and lower

* Corresponding author.
E-mail address: andre@ubi.pt (A. Silva).

https://doi.org/10.1016/j.fuel.2020.118321
Received 28 February 2020; Received in revised form 6 May 2020; Accepted 4 June 2020
Available online 29 June 2020

eccentricity values, respectively. A substantial increase in the crossflow velocity leads to aerodynamic breakup of the droplet.

1. Introduction

Energy consumption has increased twofold in the last 40 years and is expected to keep growing to fulfil global demands, causing an increase in pollutant emissions [1]. In 2017, the transport sector required a total amount of 2808 million tons of fuel equivalent, which consists of 28.9% of the total energy consumption in the world [1]. The aviation sector, in particular, operates on a fossil fuel derived product, contributing for 2% to 3% of the global carbon emissions [2]. This sector is expected to exponentially expand in order to sustain the increasing number of passengers and transported goods. With the volatility of fossil fuel prices and the increasing global awareness of greenhouse gas and pollutant emissions, the introduction of biofuels is critical in modern society. In comparison with other transport sectors, aviation imposes several restrictions in implementing any fuel contender in aviation turbines, such as interchangeability with the current operating fuels in order to avoid logistic issues, and the combustion characteristics that demand a narrow range of potential liquid fuels [2]. Among various alternative aviation fuels, hydroprocessed esters and fatty acids (HEFA) are suitable for aircraft engines, as its implementation does not require any further engine modification and does not alter the quality of the fuel [3]. The American Society for Testing and Materials (ASTM) currently allows blends of conventional jet fuel and fuels derived from HEFA in aviation turbines. According to ASTM D1655 and D7566, these blends are restricted to a maximum of 50% in volume of biofuels [4,5].

In an attempt to introduce biofuels in internal combustion engines, a fundamental study of droplet impact, in terms of atomisation, is required for further implementation. During a droplet descent and when in contact with solid surfaces, the physical and kinematic properties, surface roughness, inclination, among others, define how the phenomena will evolve in terms of the earlier impingement and later outcome. When the droplet is subjected to a continuous crossflow, in addition to the previous parameters, the deformation and secondary breakup are also factors that condition the outcome development. These phenomena occur in both nature and engineering applications, such as spray cooling and coating [6], internal combustion engines [7], ink-jet printers [8], emulsions [9], heat and mass transfer processes, etc.

Droplet impact onto dry surfaces is a widely known phenomenon and comprehensive reviews of Rein [10], Yarin [11] and Josserand and Thoroddsen [12] thoroughly detail the aspects of spreading, splashing, surface roughness and wettability, among other properties. It is characterised by several dimensionless numbers, such as the Reynolds number, $Re = U_0\rho D_0/\mu$, the Weber number, $We = \rho U_0^2 D_0/\sigma$, and the Ohnesorge number, $Oh = \mu/\sqrt{\rho\sigma D_0}$, where U_0 is the impact velocity, ρ is the density, D_0 is the initial droplet diameter, μ is the dynamic viscosity, and σ is the surface tension. These dimensionless numbers distinguish the droplet impact dynamics by relating the inertial, viscous and surface tension forces. According to Rioboo et al. [13], when a droplet contacts a dry solid surface, six distinct outcomes can be spotted: deposition, prompt and corona/crown splashing, receding breakup, rebound, and partial rebound. For low Weber and Reynolds numbers, the droplet spreads onto the surface with no production of secondary droplets. However, for higher energy impacts, prompt and crown splashing are the predominant outcomes. Prompt splash occurs for rough surfaces at earlier stages of the impact and is defined by the formation of tiny droplets that detach directly from the contact line of the lamella. Crown splash occurs for later stages when the lamella detaches from the surface, forming a crown that leads to splashing. Receding breakup, rebound and partial rebound occur mostly for non-wettable or partial wettable surfaces. These outcomes and corresponding physical/kinematic parameters assist in quantifying and establishing a splashing threshold. This threshold is commonly defined as a minimum drop velocity that leads to droplet breakup and subsequent generation of secondary droplets [14].

Šikalo et al. [15] focused their studies on oblique impact onto dry and wetted surfaces. The authors, in comparison with perpendicular droplet impact and to adapt to their current configuration, divided the droplet impact velocity onto normal (U_n) and tangential (U_t) components, and established the impact angle as the angle between the absolute velocity vector of the incident droplet and the impact surface.

The droplet deformation and breakup has been studied over the years by several authors. Guildenbecher et al. [16] define deformation as the earliest stage of secondary atomisation, where the droplet fluctuates from a spherical to an oblate ellipsoidal shape due to an unequal static pressure distribution over its surface. According to Smith and Purvis [17], droplet deformation has two temporal stages. In the first, the droplet shape is considered spherical and constant, and on the second, the airflow influences the droplet shape, distorting the interface and the air-fluid interaction becomes non-linear. The breakup phase occurs when these oscillations become unstable (vibrational breakup) and the droplet eventually shatters into secondary droplets, or when the Weber number reaches a critical value, We_c, entering the regime of bag breakup [16]. This phenomenon is characterised by the spherical droplet becoming increasingly flattened, followed by a thin hollow bag being blown downstream while attached to a more massive toroidal rim, which will subsequently burst and lead to the formation of secondary atomisation [18]. Despite the difference, many authors consider that the critical Weber number establishes the criteria for the onset of secondary atomisation. Taylor [19] theoretically investigated the rheological properties of suspended droplets dispersed in a continuous fluid. The author concluded that the droplet maintains its spherical shape if the surface tension forces are sufficient to overcome the influence of the droplet radius and the rate of distortion of the fluid. When the former exceeds the latter, the droplet breaks up, leading to secondary atomisation. Hinze [20] was one of the pioneers in theoretical and experimental work of viscous shear flow, relating types of deformation and flow patterns that might lead to breakup. Rallison and Acrivos [21] numerically studied a liquid drop of viscosity $\lambda\mu$, where λ is the viscosity ratio, under the influence of a shear flow with viscosity μ and considering interfacial surface tension with the objective of modelling the distortion and possible breakup of an initial spherical droplet as a function of time. The numerical results show that, depending on the value of Ω, which is the ratio between the flow forces and the surface tension forces, a state of equilibrium may or may not be achieved. For sufficiently strong flows, the droplet shape will be further extended to the disintegration point while, for weak flows, the droplet could relax back to an equilibrium state. Hsiang and Faeth [22] studied the droplet deformation and breakup of several fluids, such as water and solutions of glycerol, for a wide range of test conditions, in order to understand the breakup and secondary atomisation mechanisms. The initial disturbances on the droplets were generated through means of well-defined shock waves. Conclusions describe that the deformation and breakup regimes occur for $Oh < 0.1$ and for $We_g > 1$, where We_g is the Weber number based on the gas properties. Increasing Weber numbers, the following regimes were identified: no deformation, non-oscillatory deformation, oscillatory deformation, bag breakup, multimode breakup and shear breakup. For higher Ohnesorge numbers, the threshold for the deformation and breakup regimes requires a higher Weber number and, for $Oh > 4$, breakup is suppressed. Later, these

authors expanded their experimental tests for higher Ohnesorge numbers and for induced steady disturbances by high drop tube facilities in both gases and liquids [23]. Results show that substantial deformation occurs for low Ohnesorge numbers, $Oh < 0.1$, and for a Weber number of approximately $We_g = 0.6$, while the breakup regimes, such as bag, multimode and shear breakup, occur for a minimum of $We_g = 13$, $We_g = 35$ and $We_g = 80$, respectively. For high Ohnesorge numbers, $Oh > 0.1$, the tendency for the thresholds of the different regimes shifts from a constant Weber number to an approximate positive linear trend. Guido and Villone [24] focused only on the regime preceding breakup, quantitatively studying the deformation of 3D droplets under a shear flow developed by a parallel-plate apparatus. The authors investigated several parameters for analysis, such as the Capillary number, strain rates and deformation (defined by Eq. 1),

$$D = (a - b)/(a + b) \quad (1)$$

where a is the major axis and b the minor axis. Results exhibit an ellipsoidal droplet shape along three different axes for a moderate deformation range and serve as a foundation for comparison of experimental and numerical data, which were found to be in good agreement for the Capillary number range considered.

With the purpose of implementing biofuels in the civil aviation sector, this study focuses on droplets of jet fuel and biofuel mixtures under the influence of a crossflow. Therefore, the main objective of the current paper is the effect of crossflow variation on droplet deformation and outcome of a single droplet impinging onto a dry surface. To achieve that, an experimental facility was validated and experiments were made with three different fluids and five distinct crossflow velocities. The droplet characteristics, prior and during impact, were intensively investigated, including droplet deformation, eccentricity, impact angle and velocity components. The correlation of these parameters with the continuous crossflow and impact conditions aid in comprehending how droplet deformation and impact phenomena are influenced.

2. Experimental setup

Fig. 1 shows the experimental setup. It consists of a droplet dispensing system, an image acquisition arrangement, an impact surface and a wind tunnel. The droplet dispensing system includes a straight tip stainless steel needle that is connected to a syringe with a volume of 50 ml, coupled to a syringe pump which allows a pumping rate of 0.5 ml/min. The droplets leave the needle when gravity exceeds the forces due to the surface tension. The syringe pump is connected to a computer where a high-speed camera is also connected. For the image acquisition, a high-speed camera Photron FastCam mini was used. The camera was kept parallel to the falling plane of the droplet in order to fully visualise the phenomena. The motion of the droplets was pursued with 10, 000 fps (frames per second). For the impact surface, a dry smooth aluminium plate with a mean roughness of $R_a = 0.13$ μm was used. The plate roughness was evaluated with a Hommel Tester T1000 and the detailed description of the procedure is provided in [25]. This plate was equidistant of two glasses, one of them being a diffusion glass. This diffusion glass was used to provide uniform illumination and is located between the impact surface and the illumination. To intensity the contrast and to improve the phenomena visualisation, the room was completely dark and the illumination was parallel to the falling plane of the droplet. The wind tunnel exit was placed 1 cm from the droplet falling plane, and five crossflow velocities were considered.

A low speed wind tunnel produces a continuous jet flow where a single droplet is introduced and influenced by the flow field. This flow field is produced through a rig of tubes holding air forced from a driving fan. The wind tunnel has a rectangular exit nozzle with 200 × 40 mm^2. Fig. 2 shows the vertical velocity profiles measured 2 mm ahead of the wind tunnel exit nozzle. The velocity profiles were obtained through the difference between dynamic and static pressure. The probe was placed in the airflow 2 mm ahead of the wind tunnel exit nozzle and equally spaced from the vertical walls, in its vertical plane of symmetry. The crossflow velocity (U_c) was measured from its bottom to its top, being h the height of the exit nozzle, where $h = 0$ mm is the lower edge and $h = 200$ mm the upper edge. The measurements were made with gaps of 1.0 mm except when uniformity was reached. From there on it was measured with a 5.0 mm spacing until approaching the top boundary layer, returning to the gaps of 1.0 mm. The velocity profiles were normalised by the maximum crossflow velocity, U_{max}, and both uniformity and the existence of a plug flow field were verified. As stated

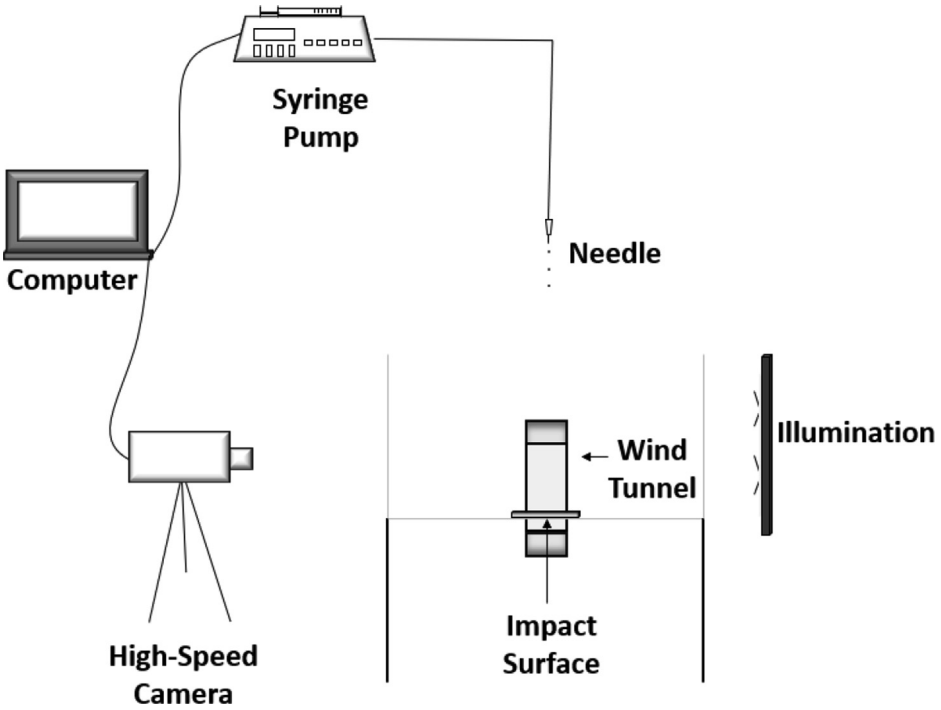

Fig. 1. Schematic of the experimental setup.

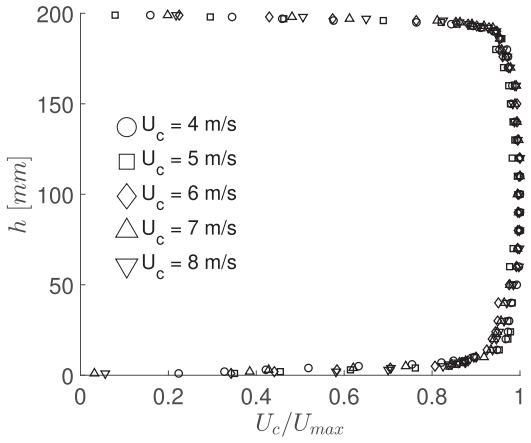

Fig. 2. Velocity profiles 2 mm after the wind tunnel exit nozzle ($U_c \pm 0.025$ m/s).

above, the aluminium plate is placed across the exit nozzle and 70 mm above its base, where the velocity profile is constant. The test cases include five different crossflow velocities: 4, 5, 6, 7, and 8 m/s. Mixtures of jet fuel and biofuel were used as working fluids. Table 1 shows the thermophysical properties of the fluids used: 100% jet fuel (JF), a mixture with 75% jet fuel and 25% biofuel, and other mixture with 50% of each type of fuel. The conventional jet fuel used is Jet A-1 and the biofuel is a hydroprocessed vegetable oil (HVO), known as NExBTL. The thermophysical properties were measured to improve the accuracy of the results [26]. The density (ρ) was obtained through the pycnometer method and decreases with the increase of biofuel percentage, however, the values between the different fuel mixtures are similar. The surface tension (σ) was measured using the pendant droplet method and the equipment used was the Data Physics – OCAH200. This property was constant for all the fluids. Ultimately, dynamic viscosity (μ) was measured with a Brookfield DV3TRVCP Rheometer with a cone and plate geometry. This is the property that varies the most within the different fluids tested, increasing with the increase of biofuel percentage.

The droplets are generated through a straight tip needle with an inner diameter of 1.5 mm, producing initial droplet diameters of 3.0 ± 0.006 mm for the 100% jet fuel and 3.1 ± 0.006 mm for the mixtures. The uncertainty values were calculated with confidence bounds of 95%. The impact velocity was changed through the droplet falling height variation. Ten experiments were made for each set of impact conditions to decrease the uncertainty and to guarantee the repeatability of the phenomena. In this away, the maximum uncertainty associated with the velocity measurements (impact velocity and its components) is ± 0.06 m/s, calculated with interval confidence of 95%. To measure these quantities, an important parameter is the pixel size, which is 0.027 mm. For the dimensionless numbers considered in this study, the maximum relative errors were calculated and displayed as follows: Weber Number (We) – 3.7%; Reynolds Number (Re) – 1.7%; Impact Angle (ϕ) – 1.1%; Eccentricity (e) – $1.6{\cdot}10^{-5}$%; Ratio of the normal velocity component to the impact velocity (U_n/U_0) – 1.7%; Ratio of the tangential velocity component to the impact velocity (U_t/U_0) – 8.8%. To perform these experiments, a strict methodology was implemented. The low speed wind tunnel was regulated in order to provide the pretended crossflow velocities. For each crossflow velocity chosen, the flow field must stabilise and evolve uniformly to assure the existence of a plug flow field when the droplet enters the crossflow. These experiments start at very low impact energies, where the only phenomenon spotted was spreading. Thenceforward, the impact energy was increased, through the variation of the impact height, until reaching the transition zone, where both spreading and splashing were visualised for the same set of impact conditions. Entering the transition zone, it was possible to identify the latest and maximum condition where 100% spreading was assured. Hereafter, the impact energy was increased to find the first condition where the occurrence of splashing is guaranteed in 100% of the cases. In summary, the maximum condition for 100% spreading, the transition zone, and the first condition for 100% splashing were identified for each crossflow velocity and for each fluid. The impact conditions tested include three different fluids and the following range of dimensionless numbers was obtained for five different crossflow velocities: $4.54{\cdot}10^{-3} < Oh < 7.28{\cdot}10^{-3}$, $2135 < Re < 4442$, and $233 < We < 484$.

3. Results and discussion

This section begins with a description of the different phenomena identified in this study. This explanation enhances the full comprehension of the following subsections. Then, the influence of the crossflow velocity variation is presented and discussed concerning the phenomena occurrence and morphology. During the development of the experiments, there are two features that stand out and reveal a strong effect upon the phenomena characterisation, namely the impact angle and droplet deformation. The influence of these two parameters on the outcomes was analysed and reported.

3.1. Phenomena description

As mentioned above, many outcomes could result from the droplet impingement upon a dry solid surface. In this study, the single droplets were exposed to the influence of continuous airflow, experiencing an aerodynamic force normal to the droplet falling motion. Due to this force, the droplet deforms and, for high crossflow velocities, breaks into a large number of secondary droplets. Several sets of impact conditions were tested in these experiments, and three different phenomena occurred: spreading, splashing, and aerodynamic breakup. Fig. 3 shows spreading (a) and splashing (b) for a droplet of 100% jet fuel influenced by a 5 m/s crossflow, where $\tau = tU_0/D_0$ is the dimensionless time and t is the time after impact. The phenomena presented for this regime correspond to the maximum limit where spreading could be reproduced with 100% accuracy for a set of impact conditions. In the first frame presented ($\tau = -0.06$), the droplet is not spherical and the deformation due to the aerodynamic force is noticeable. After the impact instant ($\tau = 0$), the fluid starts spreading radially without producing any secondary atomisation. As time evolves, the fluid continues its spreading radially along the surface ($\tau = 1.21$). In this case, the spreading is not asymmetric due to the influence of the crossflow.

On the other hand, in Fig. 3 (b) the droplet assumed a completely different shape ($\tau = -0.06$), stretching horizontally. It is believed that the droplet shape prior to impact plays an important role in the spread/splash threshold. Immediately after impact, the droplet prompt splashes ($\tau = 0.19$) and several tiny secondary droplets are ejected by the breakup of the liquid lamella, identified in frame $\tau = 0.63$. The liquid continues its spreading, extending radially. The aerodynamic force imposed by a high velocity airflow deforms the droplet and breaks apart the ligament, producing a large number of small droplets. For the higher crossflow velocity tested ($U_c = 8$ m/s), for 100% jet fuel, the droplet shape was too irregular due to the intensified deformation, and the authors decided to test a higher velocity ($U_c = 9$ m/s).

Increasing the airflow velocity led to the appearance of a new phenomenon, denominated as aerodynamic breakup [27]. Considering

Table 1
Physical properties of the fluids.

Fluid	ρ [kg/m^3]	$\sigma{\cdot}10^3$ [N/m]	$\mu{\cdot}10^3$ [Pa.s]
100% JF	798.3	25.4	1.12
75% JF/25% HVO	794.9	25.5	1.44
50% JF/50% HVO	792.3	24.6	1.79

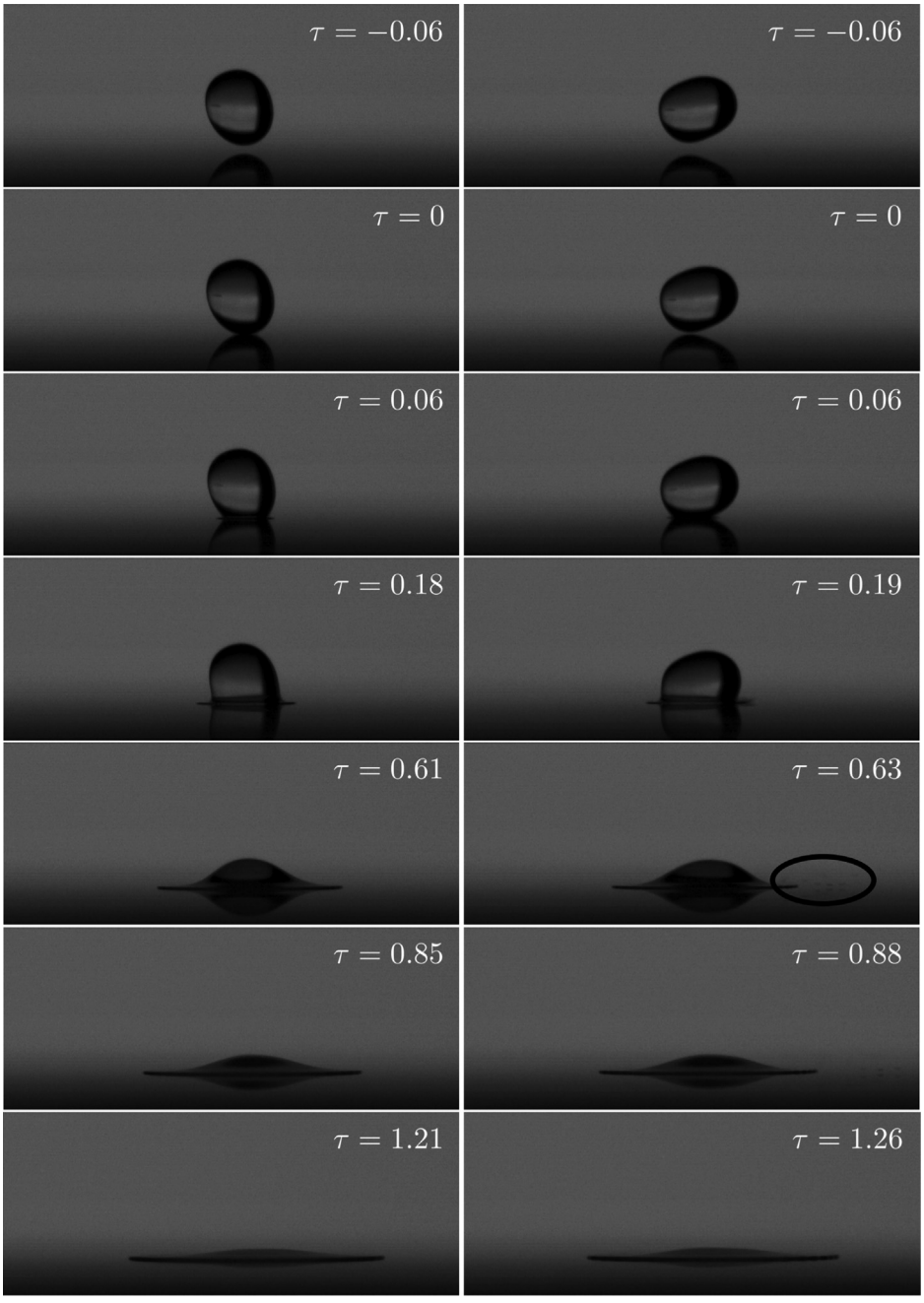

Fig. 3. Phenomenon visualisation of a 100% JF droplet (D_0 = 3.0 mm) impinging on a dry surface influenced by a continuous crossflow of U_c = 5 m/s: (a) spreading (U_0 = 1.8 m/s); (b) splashing (U_0 = 1.9 m/s).

this regime transition to breakup, it was assumed by the authors that U_c = 8 m/s is on the transition zone and, consequently, its results were not included in the analysed data. For the mixtures, the transition zone happens for U_c = 9 m/s, so the experiments for the crossflow velocity of U_c = 8 m/s were included in the data evaluation.

According to Soni et al. [27], the atomization process is inhibited by the thermophysical properties of biofuels, namely viscosity. Fuels with high viscosity usually form larger droplets, originating poorer atomization [28]. The biofuel used in this work has a high viscosity, $\mu = 3.40\ mPa.\ s$. Following this, the fuel with lower viscosity reaches the transition zone for a lower crossflow velocity than the mixtures with NExBTL, since they present a higher viscosity which will inhibit the atomisation process. Fig. 4 shows aerodynamic breakup for a droplet of 100% jet fuel influenced by a crossflow velocity of U_c = 9 m/s. Aerodynamic breakup corresponds to the droplet disintegration.

This phenomenon enlarges heat and mass transfer between the liquid and the surrounding gas, and increases surface area to volume ratio [27]. As soon as the droplet enters the crossflow, it loses its spherical shape and deforms heavily, assuming a disk-like shape. As time evolves, a thin hollow bag-like shape attached to a thick ring (toroidal ring) is formed. The bag bursts into several tiny secondary atomisation, and later, the toroidal ring breaks into large secondary droplets. This regime is called bag breakup and it is the one associated with lower Weber numbers.

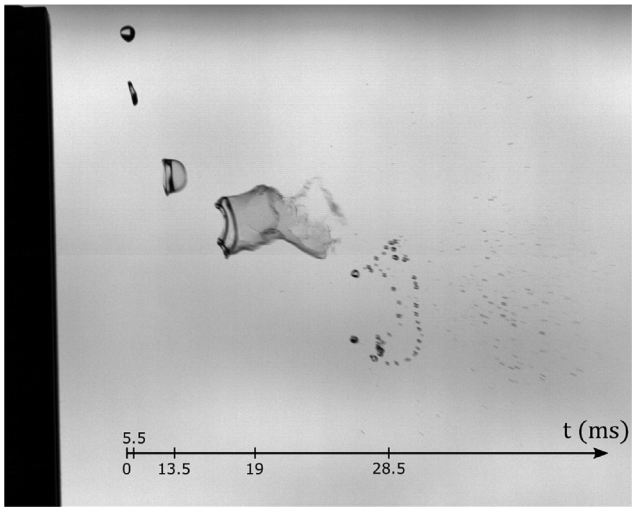

Fig. 4. Aerodynamic breakup of a 100 % JF droplet (D_0 = 3 mm) under the influence of a crossflow velocity of U_c = 9 m/s.

3.2. Influence of the crossflow upon the phenomena

One of the main goals of this study is to understand the influence of crossflow variation upon the droplet impact velocity and also upon the spread/splash transition. As explained, the methodology adopted was to identify the top limit of 100% spreading and the bottom limit of 100% splashing. Droplet impingement under the influence of a crossflow is considered an oblique impact. Thus, the droplet impacts the surface with a certain angle, and its impact velocity components must be studied. Fig. 5 shows the droplet impact velocity (U_0), its tangential (U_t) and normal (U_n) components, and the impact angle (ϕ). This angle is defined by the angle between the impact velocity and the surface.

Fig. 6 shows the variation of the tangential velocity component normalised by the droplet impact velocity depending on the crossflow velocity. The filled symbols correspond to splashing and the unfilled ones to spreading. To identify the fluids, different symbols were used to simplify the reading: circles for 100% JF, squares for 75% JF/25% HVO, and triangles for 50% JF/50% HVO. The graphic shows a clear trend, while crossflow velocity increases the tangential velocity also increases, almost linearly. The 100% jet fuel presents the lower dimensionless tangential velocity values for different crossflow velocities, while the mixtures are more influenced by the increase of the airflow. Despite having the smallest diameter, 100% jet fuel has the higher impact velocity while entering the influence of the crossflow, leading to a smaller variation in the tangential velocity component.

Fig. 7 shows the variation of the normal velocity component normalised by the droplet impact velocity depending on the crossflow velocity. This graphic follows the same nomenclature as the previous one. Due to the crossflow interaction, the normal velocity component decreases with the increase of the crossflow velocity. Entering the crossflow, the droplet earns a tangential velocity and deforms, decreasing its initial normal velocity and changing its vertical trajectory. However, analysing both graphics, it is easily perceived that tangential velocity increases at a higher scale than normal velocity decreases. It is not possible to establish a defined trend between both velocity components due to the deformation suffered by the droplet, which seems to play a major role.

Due to the wide amount of impact parameters, dimensionless numbers usually help to understand how some of them influence the outcomes. For all cases studied, the Reynolds numbers (*Re*) were calculated with the droplet properties and plotted against the crossflow velocity in Fig. 8. The Reynolds number defines the ratio between the inertial and viscous forces. Viscosity is the only thermophysical property that differs significantly between the fluids tested, being lower for 100% jet fuel and increasing with the increase of the biofuel percentage in the mixture. In this way, jet fuel presents the higher Reynolds number followed by 75% JF/25% HVO and 50% JF/50% HVO.

The Reynolds number was almost constant for the splashing cases of 100% jet fuel, and increases for 75% JF/25% HVO and 50% JF/50% HVO with the increase in the crossflow velocity. Typically, for splashing the Reynolds number is higher than for spreading due to the necessary increase of droplet impact velocity to reach the splashing regime. However, there is a case, for 100% jet fuel and U_c = 7 m/s, where spreading has a higher Reynolds number than the splashing case. At this crossflow velocity, the droplet suffers a higher deformation, changing its shape. Different shapes provide different drag coefficients. In this way, a possible explanation could be an increase in the drag force due to the droplet shape change which will affect the velocity components.

On the other hand, the Weber number (*We*) represents the ratio between inertial and surface tension forces, relating droplet kinetic and surface energy. For all cases studied, the Weber numbers were calculated and plotted against the crossflow velocity in Fig. 9. All the fluids present identical Weber numbers due to similar values of surface tension. Jet fuel presents the higher Weber number, followed by the mixtures since the droplet impact velocity presents higher values for 100% jet fuel. As can be seen, the Weber number increases with the increase of crossflow velocity for all the fluids. Similar to the Reynolds number, the Weber number is higher for splashing than for spreading due to the higher impact velocity, as mentioned above. However, there is a case, for 100% jet fuel at U_c = 7 m/s, where spreading presents a higher Weber number than the splashing case. As explained, the authors attribute that difference to the highly deformed droplet shape. Different shapes imply different drag coefficients, consequently, the drag force changes, affecting the velocity components.

3.3. Impact angle

To study the impact of a single droplet influenced by a crossflow, it is relevant to analyse the two velocity components: the normal (U_n) and tangential (U_t). The relation between these two components is the impact angle, ϕ, an important parameter for droplet impact studies. Thus, Fig. 10 shows the impact angle as a function of the crossflow velocity. Each symbol corresponds to a fluid, where the filled symbols correspond to splash and the unfilled symbols to spread. Regarding the 100% jet fuel, only four crossflow velocities were investigated due to the fact of breakup regime occurring for U_c = 9 m/s, as previously mentioned. As can be seen, increasing the crossflow velocity, the impact angle tends

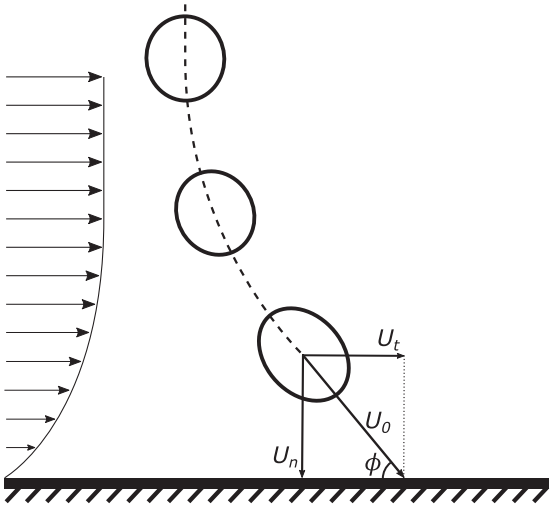

Fig. 5. Representation of the droplet impact velocity vector ($\vec{U_0}$), the correspondent normal ($\vec{U_n}$) and tangential ($\vec{U_t}$) components, and the droplet impact angle (ϕ).

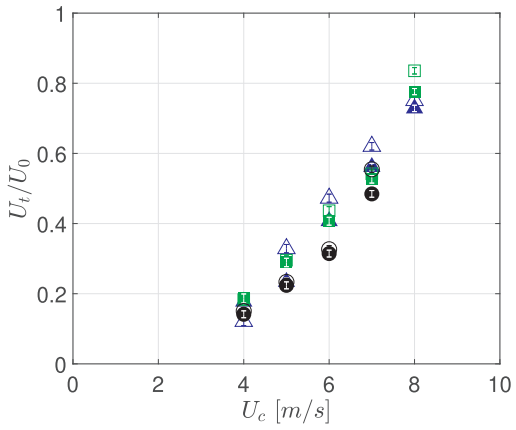

Fig. 6. Tangential velocity component normalised by the droplet impact velocity as a function of the crossflow velocity for the following conditions: ● – 100% JF, splash regime; ○ – 100% JF, spread regime; ■ – 75% JF/25% HVO, splash regime; □ – 75% JF/25% HVO, spread regime; ▲ – 50% JF/50% HVO, splash regime; △ – 50% JF/50% HVO, spread regime.

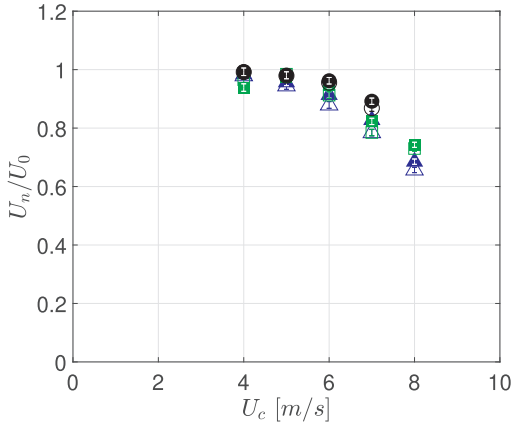

Fig. 7. Normal velocity component normalised by the droplet impact velocity as a function of the crossflow velocity for the following conditions: ● – 100% JF, splash regime; ○ – 100% JF, spread regime; ■ – 75% JF/25% HVO, splash regime; □ – 75% JF/25% HVO, spread regime; ▲ – 50% JF/50% HVO, splash regime; △ – 50% JF/50% HVO, spread regime.

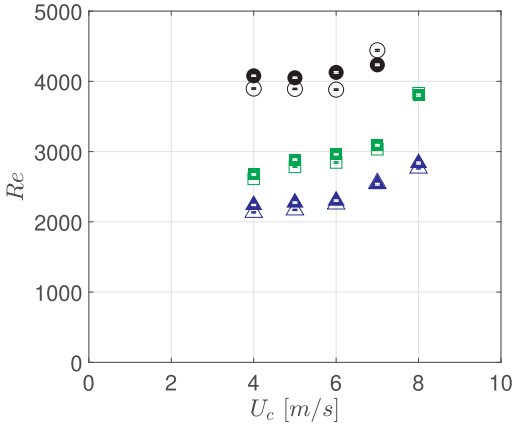

Fig. 8. Droplet Reynolds number as a function of the crossflow velocity for the following conditions: ● – 100% JF, splash regime; ○ – 100% JF, spread regime; ■ – 75% JF/25% HVO, splash regime; □ – 75% JF/25% HVO, spread regime; ▲ – 50% JF/50% HVO, splash regime; △ – 50% JF/50% HVO, spread regime.

to decrease for all the fluids, correlating with the fact that, for an increase of the crossflow velocity, the normal velocity component

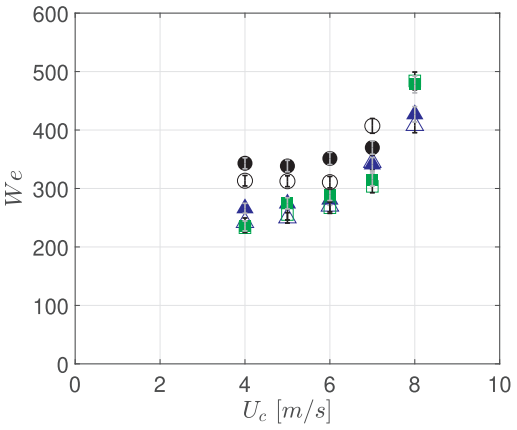

Fig. 9. Droplet Weber number as a function of the crossflow velocity for the following conditions: ● – 100% JF, splash regime; ○ – 100% JF, spread regime; ■ – 75% JF/25% HVO, splash regime; □ – 75% JF/25% HVO, spread regime; ▲ – 50% JF/50% HVO, splash regime; △ – 50% JF/50% HVO, spread regime.

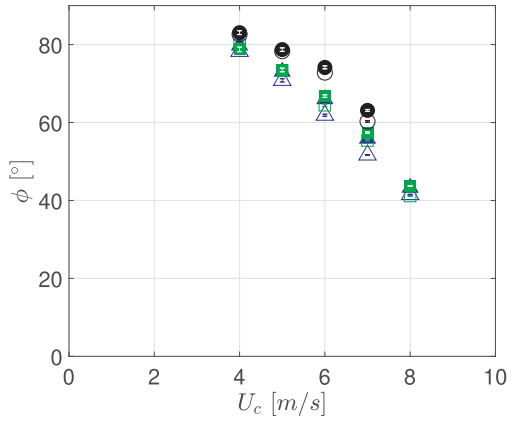

Fig. 10. Impact angle as a function of the crossflow velocity for the following conditions: ● – 100% JF, splash regime; ○ – 100% JF, spread regime; ■ – 75% JF/25% HVO, splash regime; □ – 75% JF/25% HVO, spread regime; ▲ – 50% JF/50% HVO, splash regime; △ – 50% JF/50% HVO, spread regime.

decreases while the tangential velocity component increases. The effect of the increase of tangential velocity component not only influences the impact angles, but also the droplet deformation and impact region. This observation is evident for all the fluids. Comparing the fluids, the 100% jet fuel is the fluid with the highest value at $U_c = 4$ m/s, being closer to the normal impact that occurs when $\phi = 90°$.

The lowest ϕ values correspond to the 75% JF/25% HVO and 50% JF/50% HVO mixtures at $U_c = 8$ m/s. As mentioned above, the crossflow velocity influences the droplet before impact, which promotes deformation and, for a higher airflow, it may breakup. Therefore, a relation between the impact angles and the eccentricity is shown in Fig. 11. The eccentricity, e, is a parameter used by the authors to study the droplet deformation and is represented by Eq. 2:

$$e = \sqrt{1 - \left(\frac{b}{a}\right)^2} \tag{2}$$

where a is the major axis and b the minor axis. The eccentricity parameter, e, is adopted over the deformation, D, since the former measures deviations in respect to a circumference and allows for an improved correlation of the droplet deformation and the major/minor axis of the droplet. When $0 < e < 1$, the droplet presents an elliptical shape and, for $e = 0$, the droplet is spherical.

The dashed line represented in Fig. 11 corresponds to the transition between spread and splash. The filled symbols correspond to splash, the

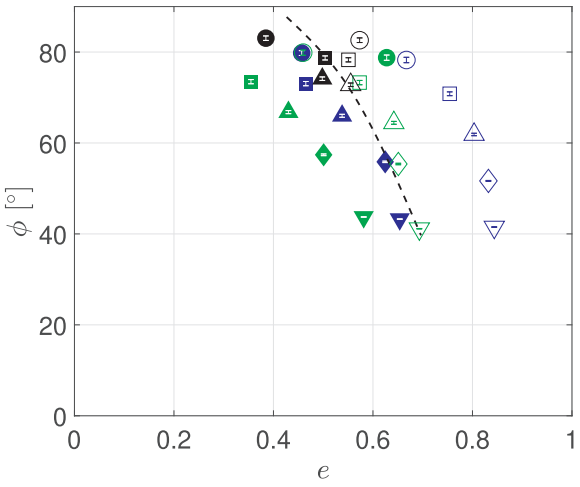

Fig. 11. Impact angle as a function of the droplet eccentricity for the following conditions: black – 100% JF; green – 75% JF/25 HVO; blue – 50% JF/50% HVO; filled symbol – splash regime; unfilled symbol – spread regime; circle – U_c = 4 m/s; square – U_c = 5 m/s; triangle – U_c = 6 m/s; diamond – U_c = 7 m/s; inverted triangle – U_c = 8 m/s.

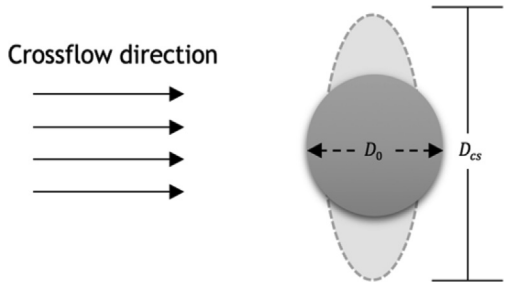

Fig. 12. Droplet deformation due to the crossflow, adapted from [16].

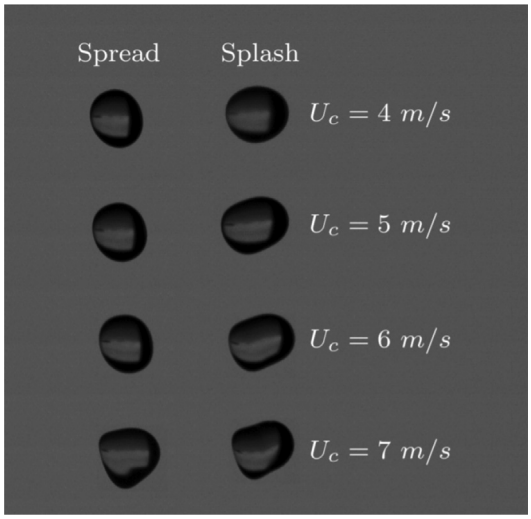

Fig. 13. Droplet deformation concerning the spread and splash regimes of 100% JF for different crossflow velocities.

unfilled symbols to spread, and each symbol corresponds to a different crossflow velocity. The splash cases are spotted on the left side of the transition zone which indicates a lower eccentricity. On the right side of the transition zone, for higher eccentricity values, spread is spotted. The increase in the crossflow velocity leads to a decrease in the impact angle and to an increase of the eccentricity values for the spread and splash regimes, which seems to be influenced by the droplet shape. For each

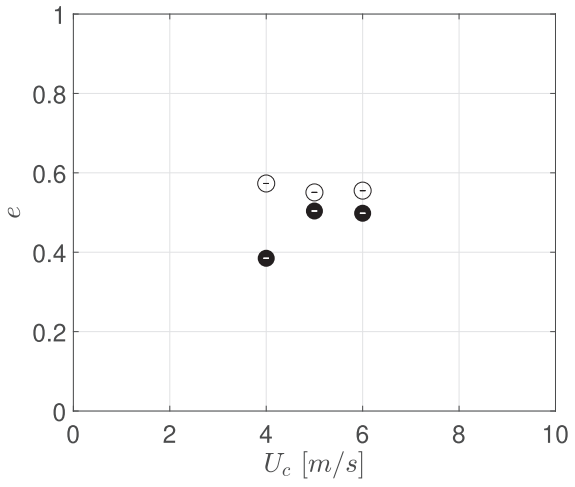

Fig. 14. Droplet eccentricity as a function of the crossflow velocity for the 100% JF and for the following conditions: ● – Splash regime; ○ – Spread regime.

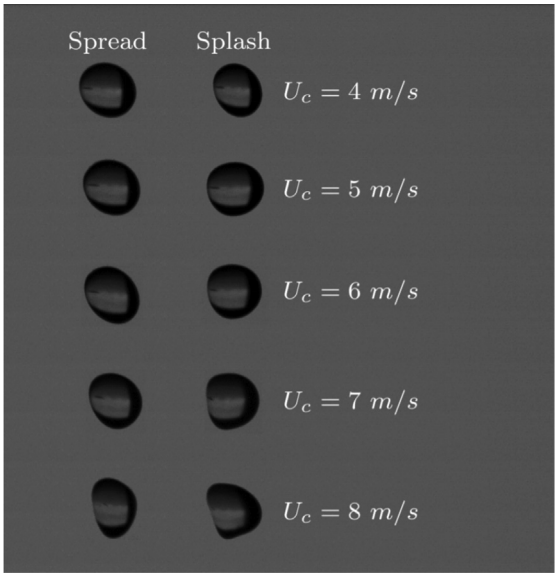

Fig. 15. Droplet deformation concerning the spread and splash regimes of 75% JF/25% HVO for different crossflow velocities.

crossflow velocity, the difference of the eccentricity values between the two phenomena is identical. This tendency is observed for all the crossflow velocities and fluids.

3.4. Droplet deformation

When a droplet is affected by a crossflow, it may deform and be oriented by the gas flow. Subsequently, the deformation is caused by an unequal static pressure distribution over the droplet surface, which varies with the crossflow velocities, as can be visualised in Fig. 12. This deformation not only promotes instabilities in the droplet surface, but also influences the obtained phenomena.

Fig. 13 displays the droplet deformation prior to impact for a 100% jet fuel droplet. For each crossflow velocity, the droplet deformation for the spread and splash regime is presented. As mentioned, the aerodynamic breakup of 100% jet fuel occurs for U_c = 9 m/s and, due to this, four crossflow velocity were studied, with the highest being U_c = 7 m/s. For the lowest crossflow velocity, U_c = 4 m/s, the spread regime presents a droplet with an elliptical shape before impact. However, for splash, the droplet seems to be more spherical. Increasing

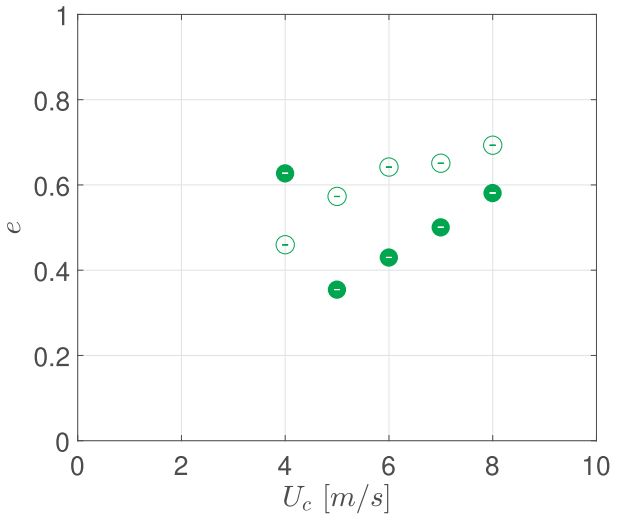

Fig. 16. Droplet eccentricity as a function of the crossflow velocity for the 75% JF/25% HVO and for the following conditions: ● – Splash regime; ○ – Spread regime.

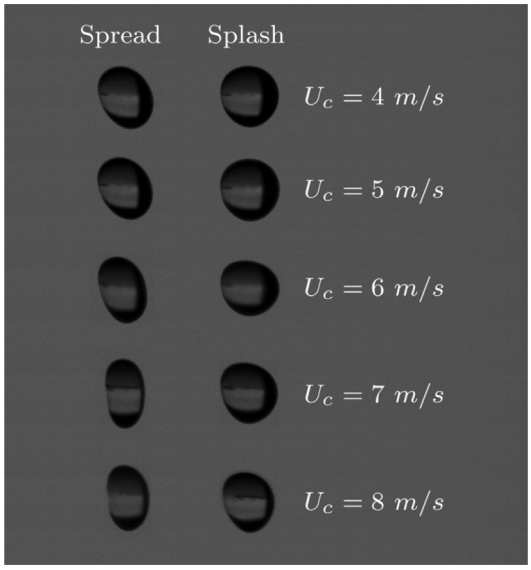

Fig. 17. Droplet deformation concerning the spread and splash regimes of 50% JF/50% HVO for different crossflow velocities.

the crossflow velocity for $U_c = 5$ m/s and $U_c = 6$ m/s, the spreading droplets present a similar shape to the spread of $U_c = 4$ m/s. On the contrary, the splash shows a droplet more deformed and not identical to $U_c = 4$ m/s. For the highest crossflow velocity, $U_c = 7$ m/s, spread and splash display a completely deformed droplet, indicating that the breakup regime is closer. To understand the relation between the droplet deformation and the phenomena obtained, a study of the eccentricity of the droplet before impact was performed. Fig. 14 shows the eccentricity of a 100% jet fuel droplet as a function of the crossflow velocity. As can be seen for the lower crossflow velocity, $U_c = 4$ m/s, the spread occurs for an eccentricity of approximately $e = 0.6$. By increasing the impact velocity, splash occurs and the droplet prior to impact is more spherical in comparison to the spread case. This can be noticed by the decrease of the eccentricity, more concretely from a value of $e = 0.6$ to $e = 0.38$. For $U_c = 5$ m/s and $U_c = 6$ m/s, the eccentricity decreases for spread and increases for splash when compared to $U_c = 4$ m/s. This fact can be observed in Fig. 13.

Fig. 15 shows the droplet deformation of 75% JF/25% HVO for five crossflow velocities. Similarly to 100% jet fuel, for $U_c = 4$ m/s, spread

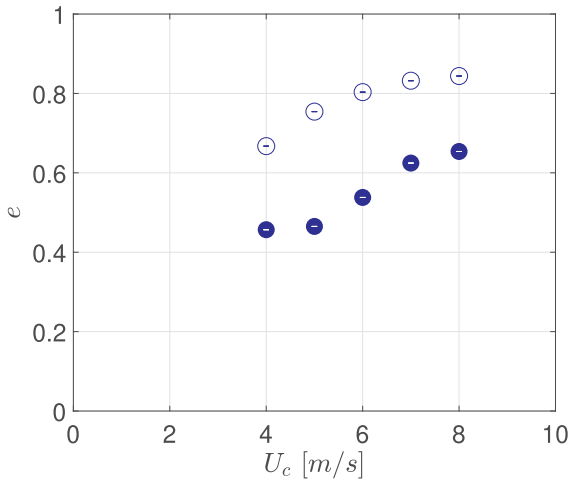

Fig. 18. Droplet eccentricity as a function of the crossflow velocity for the 50% JF/50% HVO and for the following conditions: ● – Splash regime; ○ – Spread regime.

occurs when the droplet presents an elliptical shape. On the other hand, this same shape is also noticed for the occurrence of splash. For $U_c = 5$ m/s and $U_c = 6$ m/s, elliptical and spherical shapes are noticed for the spread and splash phenomena, respectively. For $U_c = 7$ m/s, the droplet that promotes splashing is more deformed when compared to the lower crossflow velocities. This fact is more apparent for $U_c = 8$ m/s, where the droplet that corresponds to splash begins to form a bag, which indicates that it is closer to the breakup regime. Fig. 16 displays the droplet deformation in terms of eccentricity values depending on the crossflow velocity. An increase in the crossflow velocity causes an increase in the eccentricity of the droplet. This trend is noticed for the splash and spread regimes.

The maximum value for spread corresponds to $U_c = 8$ m/s, for a droplet with an eccentricity of $e = 0.69$, and the maximum value for splash occurs for $U_c = 4$ m/s, presenting an elliptical shape for an eccentricity value of $e = 0.63$. This latter value does not follow the tendency and, therefore, it would be relevant to study lower crossflow velocities ($U_c < 4$ m/s).

Fig. 17 displays the droplet shape prior to the impact of a 50% JF/50% HVO droplet influenced by a crossflow. For $U_c = 4$ m/s, $U_c = 5$ m/s and $U_c = 6$ m/s, the deformation is relatively similar, being an elliptical shape for spread and a spherical shape for splash. When the crossflow velocity increases to $U_c = 7$ m/s and $U_c = 8$ m/s, the droplet that promotes spread presents an ellipse with the major axis practically aligned with the vertical direction. On other hand, splash occurs for a droplet with more instabilities on its surface. The droplet eccentricity analysed on Fig. 18 indicates that increasing the crossflow velocity, the eccentricity of the two phenomena tends to increase. More concretely, the minimum value for eccentricity is noticed for splash with a crossflow velocity of $U_c = 4$ m/s, and the maximum value occurs for spread at $U_c = 8$ m/s. This is supported by a comparison with Fig. 17.

The analysis of the eccentricity as a function of crossflow velocity indicates that 50% JF/50% HVO is the fluid with a major difference between the eccentricity values of the spread and splash regimes. On the contrary, 100% jet fuel is the fluid that displays the minor difference between the phenomena, being more evident for higher crossflow velocities. By comparing the crossflow velocities, it was noticed that, in the presence of a high crossflow velocity, the droplets become susceptible to breakup and the deformation is clearly evident. In comparison, for lower crossflow velocities, the droplet surface does not suffer significant deformation, however there are noticeable differences in the droplet shape that influence the phenomena obtained.

4. Conclusions and future work

In the context of a wider program on biofuels in fuel mixtures for aircraft engines, the study of droplet deformation and consequent outcome due to crossflow velocity variations was considered for the present paper. Several parameters, such as droplet eccentricity, impact velocity components and impact angle were analysed for a range of impact conditions. Results show that, prior to impact, the droplet deformation is significant in defining the spread/splash threshold.

The crossflow velocity variation influences the impact velocity and, subsequently, its components. An increase in the crossflow velocity leads to an increase of the tangential velocity component and a decrease in the normal velocity component. It is also noticed that the tangential velocity component presents a higher rate of change in comparison to the normal component. Due to these reasons, spread can be spotted for higher Reynolds and Weber numbers in comparison with splashing. The influence of the crossflow on the droplet impact angle and eccentricity is also perceptible. An increase in crossflow velocity causes a decrease in the impact angle for all the fluids and an increase in the droplet eccentricity. In terms of spread/splash transition, ellipsoidal droplets promote the occurrence of spread, whereas splashing tends to occur for spherical forms, corresponding to higher and lower eccentricity values, respectively.

Future work includes a wider range of the normal velocity component, lower crossflow velocities, different biofuel percentage on the blends and identifying the distinct breakup regimes for these fluids.

Declaration of Competing Interest

The authors declare that they have no known competing financial interests or personal relationships that could have appeared to influence the work reported in this paper.

CRediT authorship contribution statement

Inês Ferrão: Methodology, Software, Formal analysis, Investigation, Writing - original draft. **Daniel Vasconcelos:** Methodology, Validation, Investigation, Writing - original draft. **Daniela Ribeiro:** Methodology, Data curation, Writing - original draft. **André Silva:** Conceptualization, Resources, Writing - review & editing, Supervision, Funding acquisition. **Jorge Barata:** Resources, Writing - review & editing, Project administration, Funding acquisition.

References

[1] I.E. Agency, Key world energy statistics 2019, 2019.
[2] Blakey S, Rye L, Wilson CW. Aviation gas turbine alternative fuels: a review. Proc Combust Inst 2011;33(2):2863–85.
[3] Hari TK, Yaakob Z, Binitha NN. Aviation biofuel from renewable resources: Routes, opportunities and challenges. Renew Sustainable Energy Rev 2015;42:1234–44.
[4] ASTM D1655-19a, Standard specification for aviation turbine fuels, ASTM International, West Conshohocken, PA (2019).
[5] ASTM D7566-19b, Standard specification for aviation turbine fuel containing synthesized hydrocarbons, ASTM International, West Conshohocken, PA (2019).
[6] Breitenbach J, Roisman IV, Tropea C. From drop impact physics to spray cooling models: a critical review. Exp Fluids 2018;59(3):55.
[7] Panão MR, Moreira ALN. Flow characteristics of spray impingement in PFI injection systems. Exp Fluids 2005;39(2):364–74.
[8] van Dam DB, Le Clerc C. Experimental study of the impact of an ink-jet printed droplet on a solid substrate. Phys f Fluids 2004;16(9):3403–14.
[9] Barnes HA. Rheology of emulsions-a review. Colloids Surf A: Physicochem Eng. Aspects 1994;91:89–95.
[10] Rein M. Drop-surface interactions vol. 456. Springer; 2014.
[11] Yarin AL. Drop impact dynamics: splashing, spreading, receding, bouncing. Annu Rev Fluid Mech 2006;38:159–92.
[12] Josserand C, Thoroddsen ST. Drop impact on a solid surface. Ann Rev Fluid Mech 2016;48:365–91.
[13] Rioboo R, Tropea C, Marengo M. Outcomes from a drop impact on solid surfaces. Atomization Sprays 2001;11(2):49–60.
[14] Yarin AL, Roisman IV, Tropea C. Collision phenomena in liquids and solids. Cambridge University Press; 2017.
[15] Šikalo Š, Tropea C, Ganić E. Impact of droplets onto inclined surfaces. J Colloid Interface Sci. 2005;286(2):661–9.
[16] Guildenbecher D, López-Rivera C, Sojka P. Secondary atomization. Exp Fluids 2009;46(3):371.
[17] Smith F, Purvis R. Air effects on large droplet impact. 4th AIAA Theoretical Fluid Mechanics Meeting. 2005. p. 5184.
[18] Pilch M, Erdman C. Use of breakup time data and velocity history data to predict the maximum size of stable fragments for acceleration-induced breakup of a liquid drop. Int J Multiphase Flow 1987;13(6):741–57.
[19] Taylor GI. The viscosity of a fluid containing small drops of another fluid. Proc R Soc London. Series A, Containing Papers Math Phys Character 1932;138(834):41–8.
[20] Hinze J. Fundamentals of the hydrodynamic mechanism of splitting in dispersion processes. AIChE J 1955;1(3):289–95.
[21] Rallison J, Acrivos A. A numerical study of the deformation and burst of a viscous drop in an extensional flow. J Fluid Mech 1978;89(1):191–200.
[22] Hsiang L-P, Faeth GM. Near-limit drop deformation and secondary breakup. Int J Multiphase Flow 1992;18(5):635–52.
[23] Hsiang L-P, Faeth G. Drop deformation and breakup due to shock wave and steady disturbances. Int J Multiphase Flow 1995;21(4):545–60.
[24] Guido S, Villone M. Three-dimensional shape of a drop under simple shear flow. J Rheol 1998;42(2):395–415.
[25] Ferrão I. Dynamic behavior of a single droplet impinging onto a sloped surface Master's thesis Universidade da Beira Interior; 2018.
[26] Ribeiro D. Experimental study of a single droplet impinging upon liquid films: Jet fuel and biofuel mixtures Master's thesis Universidade da Beira Interior; 2018.
[27] Soni SK, Kumar P, Kolhe P. High speed visualization of the bio derived fuel droplet deformation & breakup in continuous air flows. 7th International and 45th National Conference on Fluid Mechanics and Fluid Power (FMFP). 2018.
[28] Sajjadi B, Raman AAA, Arandiyan H. A comprehensive review on properties of edible and non-edible vegetable oil-based biodiesel: composition, specifications and prediction models. Renew Sustainable Energy Rev 2016;63:62–92.